CENTRE FOR INFRASTRUCTURE PERFORMANCE AND RELIABILITY

RESEARCH REPORT

Carbonation-Induced Corrosion Damage and Structural Safety for Concrete Structures under Enhanced Greenhouse Conditions

J. Peng and M.G. Stewart

Research Report No. 270.11.2008

ISBN No. 9780 9805 0355 5

THE UNIVERSITY OF
NEWCASTLE
AUSTRALIA

CARBONATION-INDUCED CORROSION DAMAGE AND STRUCTURAL SAFETY FOR CONCRETE STRUCTURES UNDER ENHANCED GREENHOUSE CONDITIONS

Jianxin Peng
Research assistant and PhD student, Institute of Bridge Engineering
Hunan University
Changsha, Hunan, 410082, China
phone: +86 731 8822221 email: pengjianxin2008@gmail.com

Mark G. Stewart
Professor and Director, Centre for Infrastructure Performance and Reliability
The University of Newcastle
New South Wales, 2308, Australia
phone: +61 2 49216027 email: mark.stewart@newcastle.edu.au

ABSTRACT

The research report will assess how predicted increases in atmospheric CO_2 levels will affect carbonation-induced corrosion damage and safety loss to RC structures, and carbonation-induced safety loss to PSC structures. Probabilistic methods are used as there is significant uncertainty and variability of atmospheric CO_2 levels, deterioration mechanisms, material properties, dimensions and loading. The time-dependent structural reliability analysis will predict the probability of corrosion initiation, the mean proportion of corrosion (cover) damage, the probabilities of flexural and shear failure of typical RC beams, and the probability of failure (collapse) of a typical prestressed concrete AASHTO bridge girder over the next 100 years considering IPCC future atmospheric CO_2 emission scenario predictions. For RC and PSC structures, for the worst case emissions scenario the mean proportion of corrosion damage is up to 540% higher than that predicted for the best CO_2 emission mitigation scenario. There is thus a significant likelihood of corrosion damage that will need costly and disruptive repairs during the service life of many concrete structures. For the worst case scenario the probabilities of flexural and shear failure are about 6% and 18% higher than the best mitigation scenario, respectively. If the worst emissions scenario is viewed as the most likely scenario, and existing design cover is less than 50-60 mm, then increasing design cover by approximately 3-18 mm may be needed to ameliorate corrosion damage over the next 100 years.

1. INTRODUCTION

It is well known that a significant threat to the performance of Reinforced Concrete (RC) and Prestressed Concrete (PSC) structures is corrosion of the embedded reinforcement. The damage caused by corrosion is, in general, difficult to assess and time consuming and expensive to repair. Furthermore, rebar corrosion in concrete has been identified as being one of the most predominant degradation mechanisms in RC structures, which seriously affects the serviceability and the safety of structures. Damage to the structure occurs in the form of concrete cracking, reduction in steel cross-section and deterioration of bond between reinforcement and concrete.[1]

The durability of RC and PSC structures is adversely affected by environmental stressors. A common and serious stressor is carbon dioxide (CO_2) which can cause depassivation of the protective film of steel reinforcement (known as carbonation). Carbon dioxide is always present in the atmosphere and its concentration is higher in the vicinity of its sources – in industrial and densely populated regions which tend to have the highest proportion of built infrastructure.

There is overwhelming evidence from laboratory and field observations of deteriorated structures that the deterioration process is spatially and time-dependent in nature. While much work has progressed on the time-dependent structural reliability of deteriorating structures.[2-4] Recent work is beginning to focus on the spatial variability of reinforced and prestressed concrete deterioration process and its effect on corrosion initiation[5], cover cracking[6-9] and strength predictions due to pitting corrosion.[10-14] Sudret et al. (2007)[9] developed spatial reliability models to predict the likelihood and extent of corrosion damage induced by carbonation, but this work assumed a constant (time-invariant) CO_2 concentration. Peng and Stewart (2008 in press)[15] used the latest CO_2 concentration data provided by the fourth assessment report of 2007 Intergovernmental Panel Climate Change (IPCC) to predict the likelihood and extent of carbonation-induced safety loss to prestressed concrete bridge girders. However, less effort has been directed to the probabilistic modelling of carbonation-induced cover cracking and structural collapse for RC structures. This is understandable as current levels of atmospheric CO_2 of about 380 ppm will, in many cases, not cause significant carbonation–induced corrosion.[16] However, climate change and global warming studies

predict that the level of atmospheric CO_2 may increase to over 1000 ppm by the year 2100.[17] As a consequence of this, carbonation may become a more critical durability issue for concrete structures in urban environments.[18]

The present paper will develop probabilistic modelling for predicting the likelihood and extent of corrosion damage and structural safety for RC and PSC structures subjected to corrosion resulting from concrete carbonation when the atmospheric CO_2 concentration increases with time over the next 100 years based on the latest Intergovernmental Panel on Climate Change (IPCC) report for climate change. Several IPCC CO_2 emission scenarios are considered. In the present paper, 'corrosion damage' refers to corrosion-induced cracking with crack width exceeding 0.3 mm. Probabilistic methods are used as there is significant uncertainty and variability of CO_2 emissions, deterioration mechanisms, material properties, dimensions and loads. A time-dependent reliability analysis is performed on typical RC and PSC beams and elements to predict: (i) probability of corrosion initiation; (ii) mean proportion of corrosion damage; (iii) probabilities of flexural and shear collapse; and (iv) proposed increases in design cover to offset any future increases in corrosion damage. The effect of concrete cover, concrete quality, corrosion rate, limit crack width and environments are considered. When combined with a life cycle cost analysis the predictive capacity of the time-dependent reliability analysis enables the extent of future repair costs to be estimated and optimal durability design specification or repair/maintenance strategies to be determined.[19]

2. TIME-DEPENDENT CO_2 CONCENTRATION

Assessing possible impacts of future climatic changes is very important in predicting the carbonation of concrete structures. The pre-Industrial Revolution level of CO_2 concentration was between 265 and 290 ppm.[20] Since the Industrial Revolution, CO_2 concentration in the atmospheric layer has been steadily increasing so that the global atmospheric concentration of CO_2 in 2000 is approximately 365 ppm.[17]

The 2007 Intergovernmental Panel on Climate Change (IPCC) reported future CO_2 concentrations for six emission scenarios.[17] The two emission scenarios considered herein are:

(i) A1FI – This scenario describes a globalised future world of rapid economic growth and the rapid introduction of new and more efficient technologies with an emphasis on fossil intensive energy consumption. This is the worst case CO_2 emissions scenario.

(ii) B1 – This scenario describes a globalised future world similar to the A1 family but with a rapid change in economic structures toward a service and information economy with reductions in material intensity and the introduction of clean and resource-efficient technologies. This is the lowest CO_2 emissions scenario.

Both these scenarios assume that there are no controls/regulations to mitigate CO_2 emissions. The annual CO_2 concentration growth-rate is 1.9 ppm per year since 2000, and so the best case scenario after 2010 would be that the CO_2 concentration is kept stable at 2010 levels (386 ppm) due to reduction and stabilisation of CO_2 emissions. This scenario is called the 'best mitigation' scenario. The fourth Assessment IPCC Report 2007 (AR4) was used for CO_2 emission scenarios for the next century.[17] The IPCC (2007) report provided information about mean CO_2 concentrations as well as confidence bounds of mean ± one standard deviation (σ). The confidence bounds take into account the predictive model inaccuracies and inherent variabilities of CO_2 emissions and predicting their effect on atmospheric CO_2 concentrations. The mean and confidence bounds for A1FI and B1 emission scenarios as well as the best mitigation scenario are shown in Fig. 1. It is observed that the standard deviation of CO_2 concentration increases with time and that the standard deviation is higher for predictions above the mean than below it.

For A1F1 emissions scenario, the standard deviations are approximated as

$$\sigma_{\text{upper}}(T) = 2.34(T - 2000) \qquad \sigma_{\text{lower}}(T) = 0.96(T - 2000) \qquad 2001 \le T \le 2100 \qquad (1)$$

where $\sigma_{\text{upper}}(T)$ and $\sigma_{\text{lower}}(T)$ are the upper and lower bound standard deviations, respectively, and T is the time from 2001 to 2100.

For B1 emissions scenario, the standard deviations are approximated as

$$\sigma_{\text{upper}}(T) = 0.78(T - 2000) \qquad \sigma_{\text{lower}}(T) = 0.39(T - 2000) \qquad (2)$$

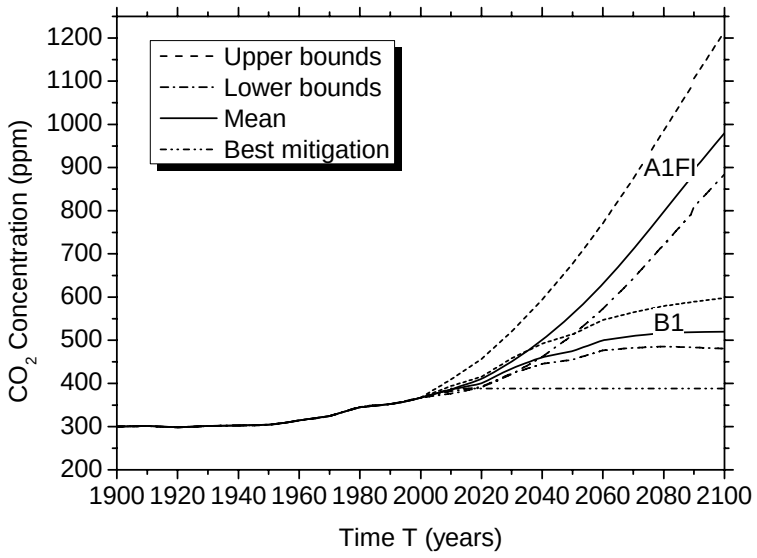

Fig. 1. Time-dependent change of atmospheric CO_2 concentration

3. TIME TO CORROSION INITIATION

The diffusion model proposed by CEB (1997)[21] and Fick's 1st law show that carbonation depth increases as a function of the square root of time. Some of the carbonation models are reviewed by Kersner et al. (1996)[22] and other models are described by Papadakis et al. (1992)[23], Yoon et al. (2007)[18], etc. However, the model proposed by Yoon et al. (2007)[18] considers a wide range of influencing parameters, but more importantly, also includes the effects of the time-dependent change in CO_2 concentration. The carbonation depth (x_c in cm) is predicted from Yoon et al. (2007)[18], but corrected to allow for modelling uncertainties as

$$x_c(t) = \mathrm{ME}_c \times \sqrt{\frac{2D_{CO_2}(t)}{a}\mathrm{ME}_{CO_2}(t)C_{CO_2}(t)t}$$

$$D_{CO_2}(t) = D_1 t^{-n_d} \qquad a = 0.75 C_e C_a O \alpha_H \frac{M_{CO_2}}{M_{C_aO}} \tag{3}$$

where ME_c is a model error for carbonation depth; $\mathrm{ME}_{CO_2}(t)$ is the time-dependent model error for CO_2 concentration with mean equal to one and variability obtained from Eqs. (1) and (2); $C_{CO_2}(t)$ is the time-dependent mass concentration of ambient CO_2 (10^{-3}kg/m^3) obtained from Fig. 1 using the conversion factor 1 ppm = 0.00188×10^{-3} kg/m^3; $D_{CO_2}(t)$ is CO_2 diffusion coefficient in concrete; D_1 is CO_2 diffusion coefficient after one year equal to 0.65, 1.24 and

2.23 for w/c of 0.45, 0.5 and 0.55 respectively; n_d is the age factor for the CO_2 diffusion coefficient equal to 0.218, 0.235 and 0.240 for w/c of 0.45, 0.5 and 0.55 respectively; C_e is cement content (kg/m^3) equal to 390, 350, and 320 for w/c of 0.45, 0.5 and 0.55 respectively; C_aO is C_aO content in cement equal to 0.60 in this paper; α_H is a degree of hydration equal to 0.71, 0.72 and 0.73 for w/c of 0.45, 0.5 and 0.55 respectively; M_{CaO} is molar mass of CaO and equal to 56 g/mol and M_{CO_2} is molar mass of CO_2 equal to 44 g/mol. As there is high variability in predicted carbonation depths, the Coefficient of Variation (COV) for ME_c is herein assumed as 0.2.

4. REDUCTION IN AREA OF REINFORCING BARS

Corrosion induced by carbonation is generally recognised as uniform corrosion resulting in a decrease in performance of RC beams that consists of approximately uniform loss of metal over the whole exposed surface of a bar.[24] Therefore, the diameter of a corroding rebar, D at time t, can be predicted directly from the corrosion current density (i_{corr}) as

$$D(t) = D_0 - 0.0232 i_{corr}(t - T_i) \qquad t \geq T_i \tag{4}$$

where D_0 is the initial diameter of the reinforcing bar (mm); T_i is the time to corrosion initiation (years); and i_{corr} is the corrosion rate (μA/cm^2).

If the reinforcement layout comprises n reinforcing bars each of diameter D_0, see Fig. 2, then the remaining cross-sectional area of reinforcing steel at time t for general corrosion of n bars is

$$A_{st}(t) = \begin{cases} \dfrac{n\pi D_0^2}{4} & 0 \leq t < T_i \\ \dfrac{n\pi\left[D_0 - D(t)\right]^2}{4} & t \geq T_i \end{cases} \tag{5}$$

It is assumed herein that general corrosion will not affect the mechanical and material properties of the steel reinforcing bar. The cross-sectional area of n uncorroded reinforcing bars is

$$A_{stnom} = n\pi \frac{D_0^2}{4} \tag{6}$$

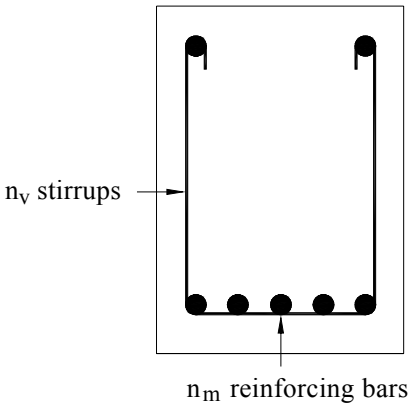

Fig. 2. Cross-section of RC beam

The carbonation–induced corrosion rate is variable and highly dependent on exposure conditions and atmospheric situations. Parameswaran et al. (2008)[25] found that the mean corrosion rate in carbonated concrete as 0.43-0.86 μA/cm^2 and 0.17 μA/cm^2 at 90-98 % and less than 85% relative humidity, respectively. The corrosion rate is 0.68 μA/cm^2 for samples moved to a carbonation chamber with a relative humidity of 65% after 3 days of exposure at 95% relative humidity.[26] According to Research Project BE 95-1347,[27] under sheltered conditions, the recommended carbonation-induced corrosion rate is 0.087 μA/cm^2 with a COV of 1.56, and under unsheltered environments the corrosion rate increases to 0.32 μA/cm^2 with a COV of 1.47. Heiyantuduwa et al. (2006)[28] measured corrosion rates in the range of 0.012-0.25 μA/cm^2 with a COV of 0.5 for 65±5% RH. Corrosion rate for carbonated mortar is as high as 0.9 μA/cm^2 when the relative humidity is more than 90%.[29] The high COV values indicate the large variability associated with corrosion rate measurements and predictions.

In the present study, corrosion rate is assumed lognormally distributed with a mean of 0.25 μA/cm^2 and a COV of 1.0 as "moderate" deterioration induced by carbon dioxide. Herein, given the large observed variability of corrosion rate, the effect of higher (0.50 μA/cm^2) and lower (0.10 μA/cm^2) corrosion rates on structural reliability will also be assessed later in the paper.

5. CORROSION-INDUCED COVER CRACKING

The corrosion-induced cover cracking occurs on the concrete surface above and parallel to the rebars. The various stages of crack growth can be described in three stages:

i) Corrosion initiation (T_i, time to corrosion initiation - carbonation reaches the surface of the reinforcing bar);

ii) Crack initiation (t_{1st}, time to first cracking - hairline crack of 0.05 mm width), and;

iii) Crack propagation (t_{ser}, time for crack to develop from crack initiation to a limit crack width, w).

5.1 Time to crack initiation

As there is a porous zone around the steel reinforcing bar the corrosion products must firstly fill this porous zone before the products start to induce internal pressure on the surrounding concrete. Therefore, some of corrosion products do not contribute to the expansive pressure on the concrete.[30] EI Maaddawy and Souki (2007)[31] divided the time between corrosion initiation and surface crack initiation into two different periods. The first one is the free expansion period for the voluminous corrosion products to fill the porous zone around the steel reinforcing bar, and the second period encompass the time in which the stress induced by corrosion products exert an expansive pressure on the concrete surrounding the steel reinforcing bar. The Liu and Weyers (1998)[32] model is a popular method for predicting time to crack initiation (t_{1st}). However, Chernin and Val (2008)[33] suggest that the derivation of a key parameter (k_p) in the Liu and Weyers model is incorrect and not solvable. Hence, the model for crack initiation in El Maaddawy and Souki (2007)[31] is used herein. The time from T_i to crack initiation is

$$t_{1st} = \left[\frac{19.5\left(D_0 + 2\delta_0\right)\left(1+\nu+\psi\right)}{i_{corr}E_{ef}}\right]\left[\frac{2Cf_{ct}}{D_0} + \frac{2\delta_0 E_{ef}}{\left(D_0 + 2\delta_0\right)\left(1+\nu+\psi\right)}\right] \tag{7}$$

where t_{1st} is the time from corrosion initiation to crack initiation (years); E_{ef} is the effective elastic modulus of concrete that is equal to $E_c/(1+\varphi_{cr})$; E_c is the elastic modulus of concrete (MPa); φ_{cr} is the concrete creep coefficient and is taken as 2.35 based on CSA Standard;[34] ν is the Poisson's ratio of concrete (0.18); f_{ct} is the tensile strength of concrete (MPa); C is the concrete cover (mm); and ψ is a coefficient equal to $D'^2/2C(C+D')$, in which $D'=D_0+2\delta_0$.

The thickness of the porous zone (δ_0) is typically in the range of 10 - 20 μm.[35] The thickness of the porous zone (δ_0) can be described using a normal distribution with mean equal to 15 μm and COV of 0.1. It should be noted, that the accuracy of the time to severe cracking is dominated by the accuracy of time to corrosion initiation (T_i) and the time since crack initiation to reach a limit crack width (t_{ser}), and so service life predictions are relatively insensitive to the crack initiation model.[8]

5.2 Time to severe cracking

The time to severe cracking referred to herein is the time when concrete cover cracking reaches a limit crack width (w). Vu et al. (2005)[36] have modelled the time to severe cracking including time-invariant and time-variant corrosion rates. In this study, corrosion rates are assumed to remain constant with time (time-invariant). Therefore, a model proposed by Vu et al. (2005)[36] that the time from corrosion initiation to propagate to a limit crack width (w) in real RC structures (in years) is

$$T_{sp} = t_{1st} + t_{ser} \approx t_{1st} + k_R \times \frac{0.0114}{i_{corr}} \left[A\left(\frac{C}{w/c}\right)^B \right] \qquad 0.3 \text{ mm} \le w \le 1.0 \text{ mm} \tag{8}$$

where

$$k_R \approx 0.95 \left[\exp\left(-\frac{0.3 i_{corr(exp)}}{i_{corr}} \right) - \frac{i_{corr(exp)}}{2500 i_{corr}} + 0.3 \right] \qquad k_R \ge 0.2 \tag{9}$$

and where T_{sp} is the time from corrosion initiation to severe cracking (years); w/c is the water cement ratio; A and B are empirical constants and k_R is a rate of the loading correction factor where $i_{corr(exp)}$ is the accelerated corrosion rate used to derive constants A and B. In the present case $i_{corr(exp)}$=100 μA/cm^2 and A=65 and B=0.45 for w=0.3 mm and A=225 and B=0.29 for w=1.0 mm. The model is valid for 16 mm diameter bars. Model errors for Eq. (8) are described in Table 2.

The rate of crack propagation seems to increase as the reinforcing bar diameter increases.[37,38] However, the crack propagation data shows 'relatively significant scatter' so an accurate predictive model of the effect of bar diameter on crack propagation (t_{ser}) is not available.[37] Accelerated corrosion tests at The University of Newcastle show that increasing the bar diameter from 16 mm to 27 mm reduces t_{ser} by 12% to 32%.[38] A model by Vidal et al.

(2004)[37] predicted a 30% to 40% decreases in t_{ser} if bar diameter increases from 16 mm to 27 mm. If bar diameter reduces from 16 mm to 10 mm, then Vidal et al. (2004)[37] predicted a 40% to 60% increase in t_{ser}. In the absence of the other data or models, it is assumed herein that for a 10 mm diameter bar the t_{ser} given by Eq. (8) is increased by 50% and for a 27 mm diameter bar the t_{ser} given by Eq. (8) is reduced by 25%.

6. TIME-DEPENDENT RELIABILITY ANALYSIS

6.1 Limit states

The corrosion initiation limit state will take place when the carbonation depth reaches the surface of the reinforcing bar and this limit state can be represented as

$$G_{\mathrm{CI}}(X) = C - x_c(t) \tag{10}$$

where $x_c(t)$ is the carbonation depth at time t obtained from Eq. (3).

The cumulative probability of corrosion initiation at time t is

$$p_{\mathrm{ci}}(t) = \Pr\left[G_{\mathrm{CI}}(X) \le 0\right] \tag{11}$$

where G_{CI} is the time to corrosion initiation limit state function given by Eq. (10).

In this study corrosion damage is defined as the time when concrete cover severely cracks. Therefore, the corrosion damage limit state is

$$G_{\mathrm{S}}(w,t) = \left(T_{\mathrm{i}} + T_{sp}\right) - t \tag{12}$$

where T_{i} is the time to corrosion initiation; and T_{sp} is the time to excessive cracking which is the time for a crack to propagate from corrosion initiation to a limit crack width (w).

The cumulative probability of corrosion damage at time t is

$$p_{\mathrm{S}}(w,t) = \Pr\left[G_{\mathrm{S}}(w,t) < 0\right] \tag{13}$$

A method proposed by Sudret et al. (2007)[9] is used herein to calculate the mean proportion of corrosion damage is

$$\bar{\mathrm{d}}_{\mathrm{crack}}(w,t) = p_{\mathrm{S}}(w,t) \times 100\% \tag{14}$$

where $p_s(w,t)$ is the probability of corrosion damage given by Eq. (13). Note that Eq. (14) is only appropriate for homogeneous structures (i.e. spatial variability is ignored).

The reinforcement layout for a typical singly reinforced RC beam is shown in Fig. 2. Strength prediction models used herein are based on yield capacity as these have been verified when predicting ultimate capacity for corroded RC beams.[24] The ultimate flexural capacity (M_u) of a singly reinforced RC beam is

$$M_{\mathrm{u}} = \mathrm{ME} \times A_{\mathrm{st}} f_y \left(d - \frac{A_{\mathrm{st}} f_y}{1.7 f_c' b} \right) \tag{15}$$

which is a function of model error (ME), concrete compressive strength (f'_c-MPa), effective depth (d-mm); beam width (b-mm), yield stress (f_y-MPa) and cross-sectional area of reinforcement (A_{st}-mm^2).[39]

The ultimate shear capacity for beams with shear reinforcement (V_u) comprises the shear capacity of concrete (V_c) and shear reinforcement (V_s):

$$V_u = V_c + V_s \tag{16}$$

where

$$V_c = \mathrm{ME}_{\mathrm{sc}} \times 0.17 \sqrt{f_c'} bd \tag{17}$$

$$V_s = \mathrm{ME}_{\mathrm{ss}} \times \frac{A_{\mathrm{v}} f_{yd}}{s} = \mathrm{ME}_{\mathrm{ss}} \times n_{\mathrm{v}} A_{\mathrm{v}} f_y \tag{18}$$

where A_v is the cross-sectional area of shear reinforcement (stirrup) with spacing s[39]; n_v is the number of stirrups and ME_{sc} and ME_{ss} are model errors.

The flexural capacity ($M(t)$) of a singly reinforced RC beam at time t is approximated as

$$M(t) = \frac{A_{\mathrm{st}}(t)}{A_{\mathrm{stnom}}} M_{\mathrm{u}} \tag{19}$$

where $A_{st}(t)$ is obtained from Eq. (5) for n=n_m reinforcing bars.

The shear capacity ($V(t)$) of a singly reinforced RC beam at time t is also approximated as

$$V(t) = V_c + \frac{A_{\mathrm{st}}(t)}{A_{\mathrm{stnom}}} V_{\mathrm{s}} \tag{20}$$

where $A_{st}(t)$ is obtained from Eq. (5) for n=n_v stirrups.

The strength limit state is exceeded when actual load effects exceed resistance. In general, if it is assumed that k load events S occur within the time interval (0, t) at times t_i (i =1, 2,…, k) and so this limit state can be represented as

$$G_{\mathrm{M}_{t_i}}(X) = M(t_i) - S_{\mathrm{m}}(t_i) \qquad G_{\mathrm{V}_{t_i}}(X) = V(t_i) - S_{\mathrm{v}}(t_i) \tag{21}$$

where $M(t_i)$ is the structural flexural resistance at time t_i; $S_m(t_i)$ is the flexural load effect at midspan at time t_i; $V(t_i)$ is the structural shear resistance at time t_i; and $S_v(t_i)$ is the shear load effect at time t_i. The cumulative probabilities of flexural and shear failure anytime during the time interval (0, t) are

$$p_{\mathrm{fM}}(t) = 1 - \Pr(G_{\mathrm{M}_{t_1}} > 0 \cap G_{\mathrm{M}_{t_2}} > 0 \cap \cdots \cap G_{\mathrm{M}_{t_k}} > 0)$$

$$p_{\mathrm{fV}}(t) = 1 - \Pr(G_{\mathrm{V}_{t_1}} > 0 \cap G_{\mathrm{V}_{t_2}} > 0 \cap \cdots \cap G_{\mathrm{V}_{t_k}} > 0) \tag{22}$$

For deteriorating structures the deterioration process will reduces structural resistance and so structural resistance is time-dependent. This is a first passage probability.

Spatial effects for geometric and physical parameters known to influence structural reliabilities are not considered for general corrosion as their inclusion will be less important as it is for chloride-induced pitting corrosion.[7,10] However, inclusion of spatial variability of environment, dimensions and material properties is an area for further research.

6.2 Computational procedure

The time-dependent reliability analysis of this study is complicated since it involves a large number of random variables and dependent variables. For example, concrete compressive strength, CO_2 concentration, structural dimensions, corrosion rate, etc. are random variables whereas concrete tensile strength and modulus of elasticity of concrete are dependent variables. Therefore, closed-form solutions are not tractable and so Monte-Carlo simulation is used as a computational method for the time-dependent reliability analysis.

Monte-Carlo simulation is uses herein to evaluate Eqs. (11), (14) and (22). For each simulation run, the carbonation depth, time to corrosion initiation and corresponding

remaining cross-sectional areas of reinforcing bars are inferred from Eqs. (3)-(5). The time to crack initiation and time to excessive cracking are inferred from Eqs. (7)-(9). The flexural resistance at the midspan and shear resistance at the support of the same beam are then calculated at each time interval. Note that corrosion of each reinforcing bar is fully correlated. The applied loads are then randomly generated for the time increment and the peak load effects calculated. The limit state functions Eqs. (10), (12) and (21) are then checked. This process continues for successive annual time increments failure occurs ($G < 0$) or its service life is reached. At the completion of all simulation runs, the cumulative probability of corrosion initiation (Eq. (11)), the mean proportion of corrosion damage (Eq. (14)), and the cumulative probabilities of flexural and shear failure (Eq. (22)) are inferred at each time increment. Note that the CO_2 concentration is fully correlated with time.

7. STRUCTURAL EXAMPLE – RC BEAM

7.1 RC floor beam

The structural configuration is a RC beam with cross section given by Fig. 2. The nominal (or design) capacity of an uncorroded RC beam is denoted as M_{nom} and V_{nom} for flexure and shear, respectively. In the present case, the nominal resistance for a RC beam is obtained from the design condition $\phi R_{\text{nom}}=1.2G_{\text{n}}+1.6Q_{\text{n}}$,[39] in which $\phi=0.9$ and $\phi=0.75$ for flexure and shear, respectively. It follows that nominal flexural and shear capacity is $M_{\text{nom}}=(1.2G_{\text{n}}+1.6Q_{\text{n}})/0.9$ and $V_{\text{nom}}=(1.2G_{\text{n}}+1.6Q_{\text{n}})/0.75$, respectively. The nominal capacity depends on the live-to-dead load ratio $\rho = Q_{\text{n}}/G_{\text{n}}$ where G_{n} and Q_{n} are design dead and live loads respectively. For shear design, the ratio $V_{\text{c}}/V_{\text{s}}$ is used to denote the ratio of nominal concrete (V_{cnom}) to reinforcement shear (V_{snom}) capacities.

The ultimate to nominal flexural resistance ($M_{\text{u}}/M_{\text{nom}}$) for a RC beam is modelled as a normal distribution with mean of 1.135 and COV of 0.085.[40] These flexural statistics include the random variability of ME, f'_{c} , d , f_y , and A_{st} in Eq. (15). The ultimate to nominal shear resistance provided by concrete ($V_{\text{c}}/V_{\text{cnom}}$) is normally distributed with mean of 1.22 and COV of 0.20.[40] The ultimate to nominal shear resistance provided by shear reinforcement ($V_{\text{s}}/V_{\text{snom}}$) is obtained from Nowak et al. (2005)[40] as normally distributed with mean of 1.20 and COV of 0.15. These shear statistics include the random variability of ME_{cs}, ME_{ss}, f'_{c} , b, s, f_y and A_{v} in

Eqs. (17) and (18). The reduction in bond between concrete and steel is ignored herein. For general corrosion the proportional loss of V_s is not affected by stirrup spacing s/d ratio.

Statistical parameters for a stochastic office floor load are shown in Table 1. The load effects form these uniformly distributed loads produce a bending moment (S_m) and shear force (S_v). The time period is taken as 100 years, with extraordinary live load effects updated annually and sustained live load effects updated every 8 years resulting in k=100 load events.

Load	Duration	Mean	COV	Distribution	References
Dead load	Permanent	$1.05G_n$	0.1	Normal	[41]
Live load					
Sustained	8 Years	$0.30\ Q_n$	0.60	Gamma	[42]
Extraordinary	1 Year	$0.19\ Q_n$	0.66	Gamma	[43]

Note: G_n and Q_n design loads specified from ANSI/ASCE 7-93 (ANSI/ASCE 7-93 (1994))[44].

Table 1. Load Model Statistics

The bottom main longitudinal and transverse reinforcement is 16-mm or 27-mm diameter bars and stirrups are 10-mm reinforcement. The specified concrete compressive strength is 30 MPa and water-cement ratio is 0.5. In the present analysis, concrete design cover is 30 mm which is used for many building structures such as internal structural members and wall panels for building facades under non-marine environments in many countries including the UK,[45] Europe, [46] U.S.,[39] Australia[47] and China[48]. The live-to-dead load ratio (ρ = 0.5-1.5) did not affect the overall trend of the results presented herein, hence results to follow are for ρ =1.0. The mean corrosion rate is 0.25 μA/cm^2. The likelihood and extent of corrosion initiation, corrosion damage and strength failure of RC beams will be evaluated at annual time increments for a design life of 100 years. The purpose of the example is to model a continuous deterioration process (no inspection or maintenance). The statistical parameters for model errors, corrosion parameters, material properties and dimensions are listed in Table 2.

Parameters			Mean	COV	Distribution	References
f'_{cyl} concrete cylinder strength			F'_c[a] + 7.5 MPa	σ = 6 MPa	Lognormal	[49]
k_w ($f'_c = k_w f'_{cyl}$)		Poor	0.53	0.08	Normal	[49]
		Fair	0.86	0.06	Normal	[49]
		Good	1.00	0.0	Normal	[49]
Model errors	CO_2 concentration (ME_{CO_2})		1.0	Eqs.(1), (2)	Normal[b]	
	Carbonation depth (ME_c)		1.0	0.20	Normal	
	T_{sp}	w=0.3 mm	1.09	0.19	Normal	[8]
		w=1.0 mm	1.05	0.20	Normal	[8]
Cover			C_{nom} +1.6 mm	σ = 11.1 mm	Normal	[50]
$f_{ct}(t)$			$0.53(f_c(t))^{0.5}$	0.13	Normal	[51]
$E_c(t)$			$4600(f_c(t))^{0.5}$	0.12	Normal	[51]
i_{corr} (μA/cm^2)			0.1, 0.25, 0.50	1.0	Lognormal	
δ_0 (μm)			15	0.1	Normal	

a, F'_c = specified concrete compressive strength; b, truncated at 380 ppm.

Table 2. Statistical Parameters for Corrosion Parameters, Material Properties and Dimensions

7.2 Results

7.2.1 Corrosion initiation

The mean carbonation depths under ambient environments for A1FI, B1 and Best mitigation scenarios and 0.5 w/c ratio are 20.3 mm, 14.4 mm, and 12.1 mm after 100 years, respectively. The COV for carbonation depth increases with time from 0.20 to 0.22. For the worst case scenario (A1FI) the carbonation depth is 53% higher than that for the best mitigation scenario. This shows that future emission scenarios induced by economic development and population growth affects concrete carbonation and thus the onset of corrosion of reinforcing bars. Fig. 3 shows the probabilities of time to corrosion initiation for all emission scenarios. As seen in Fig. 3, probabilities of corrosion initiation increase as the CO_2 concentration increases. For the worst case scenario (A1FI) the probability of corrosion initiation is up to 720% higher than that predicted for the best mitigation scenario for 30 mm cover and w/c= 0.5. If design cover is increased to 40 mm the probabilities of corrosion initiation reduces significantly to no more than 0.034.

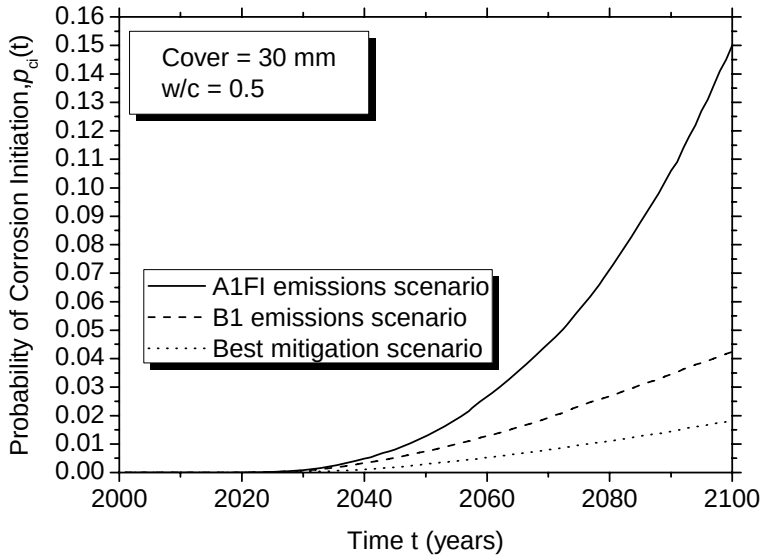

Fig. 3. Probabilities of corrosion initiation, for 30 mm cover and w/c=0.5

7.2.2 Corrosion damage

Fig. 4 shows the mean proportions of corrosion damage ($\bar{d}_{crack}(w,t)$) for RC structures. For the first 30-40 years of service life the effect of carbonation on structural reliability is negligible. However, for the worst case scenario (A1FI) and Y16 diameter bar the mean proportion of corrosion damage is up to 540% higher than that observed for the best mitigation scenario for 30 mm cover and w/c=0.5 experiencing 1 mm crack widths. This indicates the higher CO_2 concentration could lead to a significant likelihood and extent of corrosion damage that will need costly and disruptive repairs during the service life of many concrete structures. For the Y27 diameter bar the mean proportion of corrosion damage is about 13% and 46% higher than that predicted for the Y16 and Y10 diameter bars under A1FI emissions scenario for 30 mm cover and w/c=0.5, respectively. This shows that a larger bar diameter will result in a corresponding higher likelihood of corrosion damage. However, the influence of diameter bar reduces as the atmospheric CO_2 concentrations decrease.

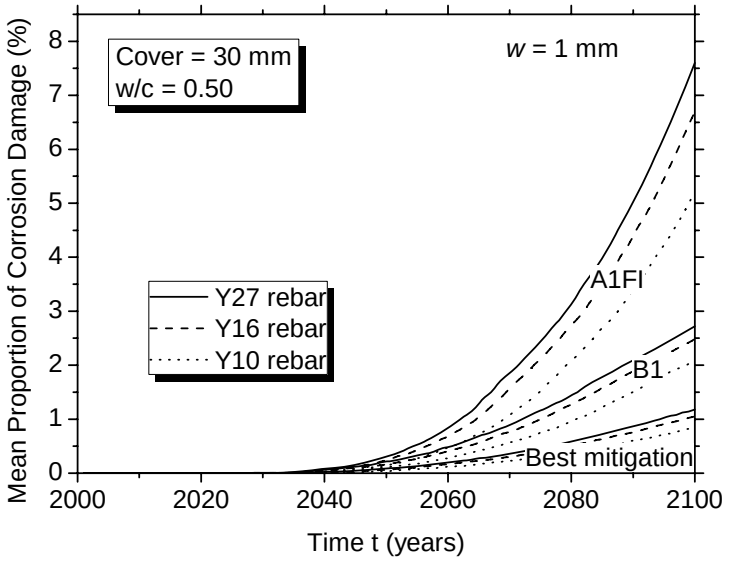

Fig. 4. Mean proportions of corrosion damage, for 30 mm and w/c=0.5

7.2.3 Structural (Strength) failure

Fig. 5 shows the probabilities of failure for RC office floor beams, for 30 mm cover and w/c=0.5 for all emission scenarios. For comparative purposes, failure probabilities for the ideal case of no deterioration are shown also. For the first 50-80 years of service life the effect of carbonation on structural reliability is negligible. However, for the worst case scenario (A1FI) and Y10 stirrups the probability of shear failure is about 18% higher than for best mitigation and V_c/V_s=1.0 after 100 years of service life. For Y16 reinforcement the probability of flexural failure is only 6% higher than that observed for the best mitigation scenario after 100 years. It is observed from Fig. 5(a) that the probability of shear failure decreases as the V_c/V_s ratio decreases. Moreover, as the V_c/V_s ratio reduces the effect of reinforcement corrosion on shear capacity increases resulting in a significant proportional increase in the probability of shear failure. With reference to Fig. 5(c), for Y27 reinforcement there is negligible influence of CO_2 concentration on the probability of flexural failure. This is because larger bars have smaller proportional corrosion loss. Note that the reliability index (β) after 50 years for flexure, assuming no deterioration, is 3.50. This is consistent with target reliability indices for RC members for buildings and bridges, and shows that the resistance and loading modeling is consistent with that experienced by RC members in general.

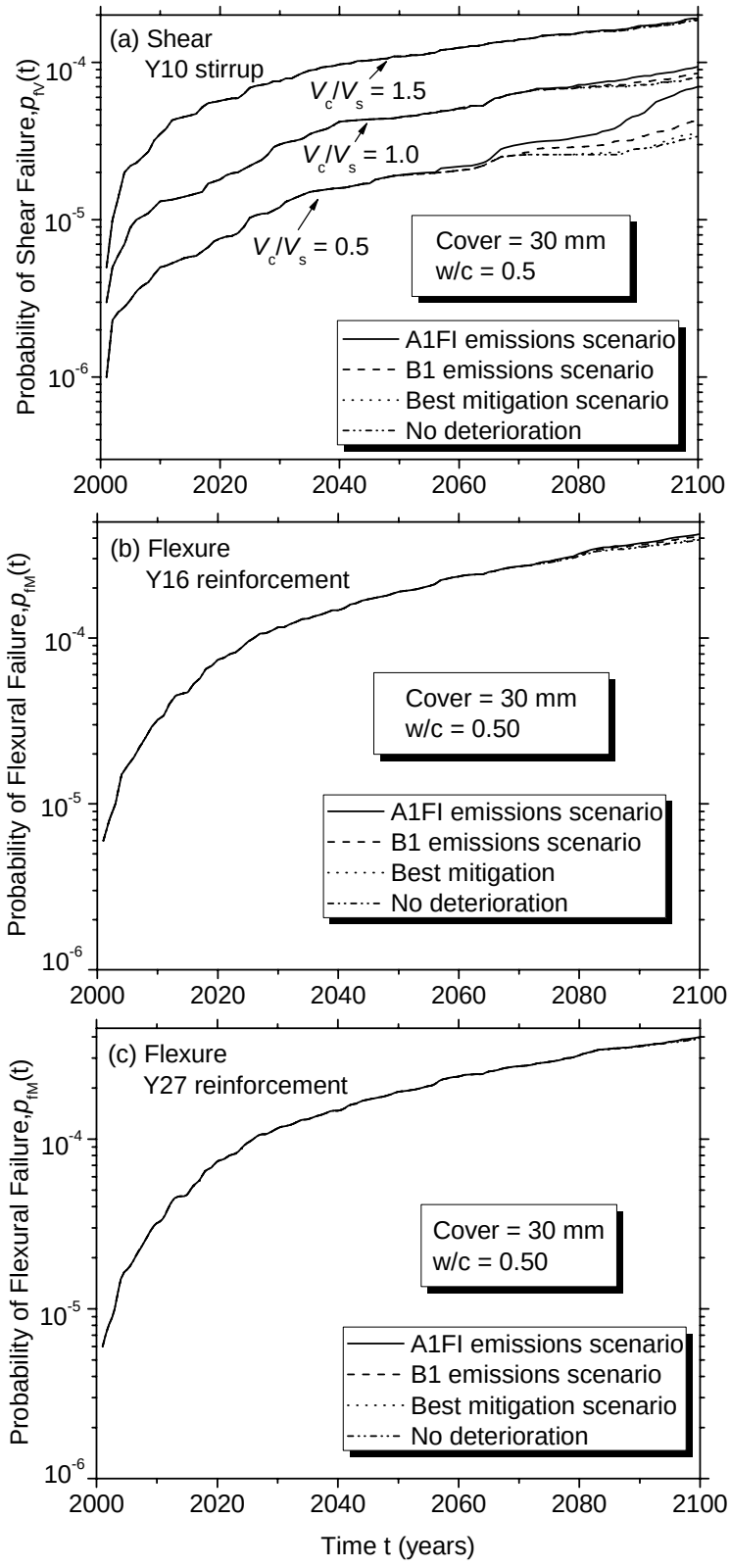

Fig. 5. Probabilities of failure for RC office floor beams, for 30 mm cover and w/c=0.5

7.2.4 Influence of cover and w/c ratios on corrosion damage

The emission scenarios in Fig. 1 are now used to assess the mean proportions of corrosion damage considering changes in design cover and w/c ratio. The RC structure is exposed to an atmospheric environment with a typical corrosion rate of 0.25 μA/cm^2. Three durability specifications are considered:

(i) Poor: cover=20 mm, w/c= 0.55;

(ii) Fair: cover=30 mm, w/c= 0.50;

(iii) Good: cover=40 mm, w/c= 0.45.

Fig. 6 shows the influence of durability design specifications on the mean proportions of corrosion damage for Y16 reinforcement, w=1 mm, and for all emission scenarios and various covers and w/c ratios. It is observed that for good durability design specification the mean proportion of corrosion damage is only 0.3% and so corrosion damage induced by carbonation is negligible. However, for a poor durability design specification, the mean proportions of corrosion damage are quite high. For example, even after 50 years there is a 18% chance of corrosion damage. This mean proportion can increases to nearly 37% after 100 years – a significant likelihood of corrosion damage that will need costly and disruptive repairs. It is observed from Fig. 6 that poor durability specifications significantly increase the likelihood and extent of corrosion damage. If the limit crack width is reduced to w=0.3 mm then the mean proportion of corrosion damage increases by approximately 25% to 70%.

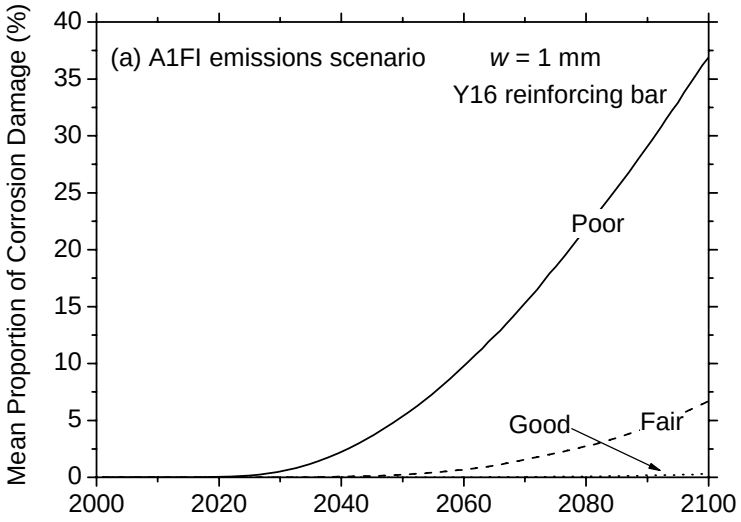

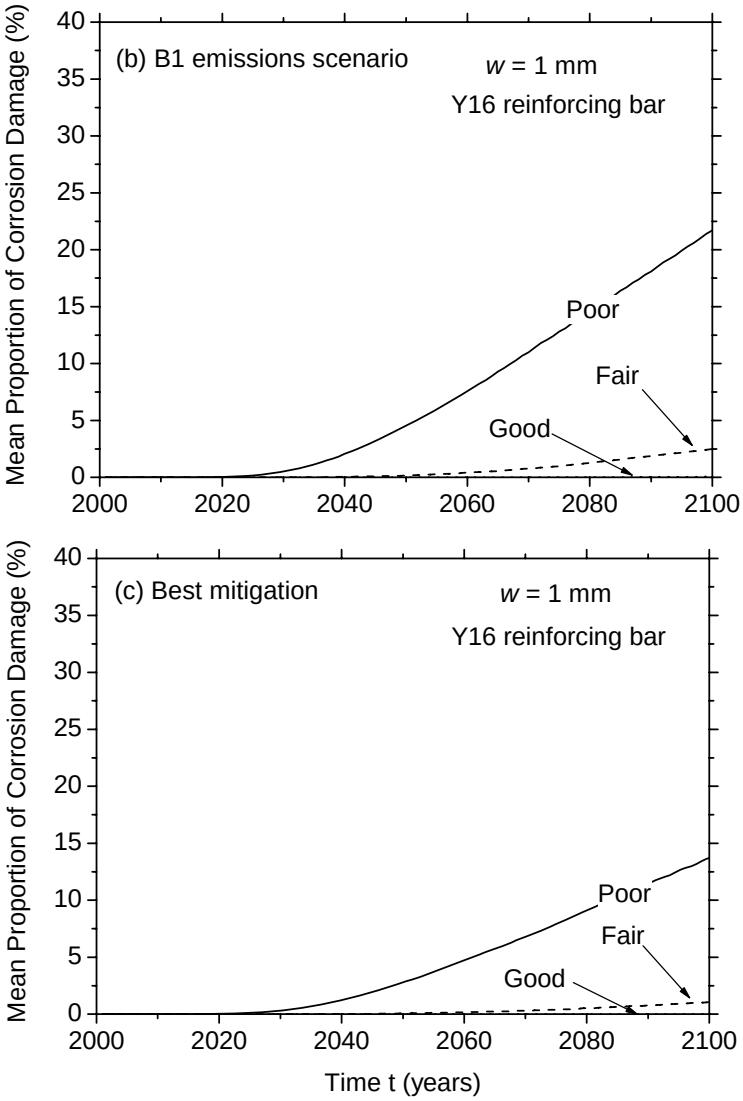

Fig. 6. Mean proportions of corrosion damage, for various covers and w/c ratios

7.2.5 Effect of corrosion rate

The carbonation-induced corrosion rate is highly dependent on ambient environments. Three mean corrosion rates, representing three deterioration situations, are used.

(i) i_{corr}=0.10 μA/cm^2;

(ii) i_{corr}=0.25 μA/cm^2;

(iii) i_{corr}=0.50 μA/cm^2.

Fig. 7 shows the mean proportions of corrosion damage for various corrosion rates, for the worst emissions scenario. It is observed from Fig. 7 that for mean i_{corr}=0.50 μA/cm^2 the mean

proportion of corrosion damage is up to 160-280% higher than that observed for mean i_{corr}=0.10 μA/cm^2 for various bar diameters over the next 100 years.

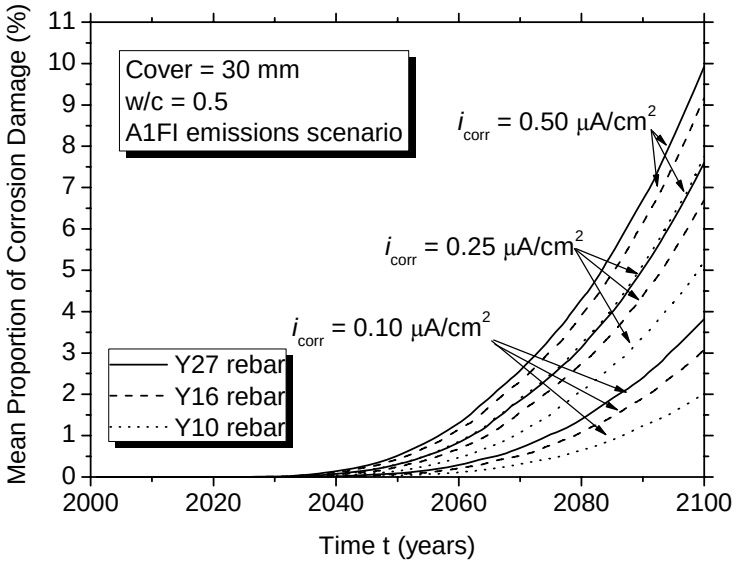

Fig. 7. Mean proportions of corrosion damage, for various corrosion rates

Fig. 8 shows the probabilities of failure for various corrosion rates, for the worst emissions scenario. It is found that for mean i_{corr}=0.50 μA/cm^2 the probability of shear failure (V_c/V_s=1.0) is up to 120% higher than that for mean i_{corr}=0.10 μA/cm^2 for Y10 stirrups over the next 100 years. It is also found that for mean i_{corr}=0.50 μA/cm^2 the probability of flexure failure is 67% higher than that observed for mean i_{corr}=0.10 μA/cm^2 for Y16 reinforcing bars over the next 100 years. If Y27 reinforcement is used then the change in corrosion rate has a negligible effect on probabilities of flexural failure. Therefore, effective measures used to inhibit the corrosion rate can mitigate the extent of corrosion damage and structural collapse probabilities. However, if concrete cover is increased to 40 mm then even if mean i_{corr}=0.50 μA/cm^2 the probabilities of flexural and shear failures are similar to that for no deterioration. Clearly, the effect of carbonation-induced corrosion for RC beams with covers of 40 mm or more is negligible for flexural and shear limit states.

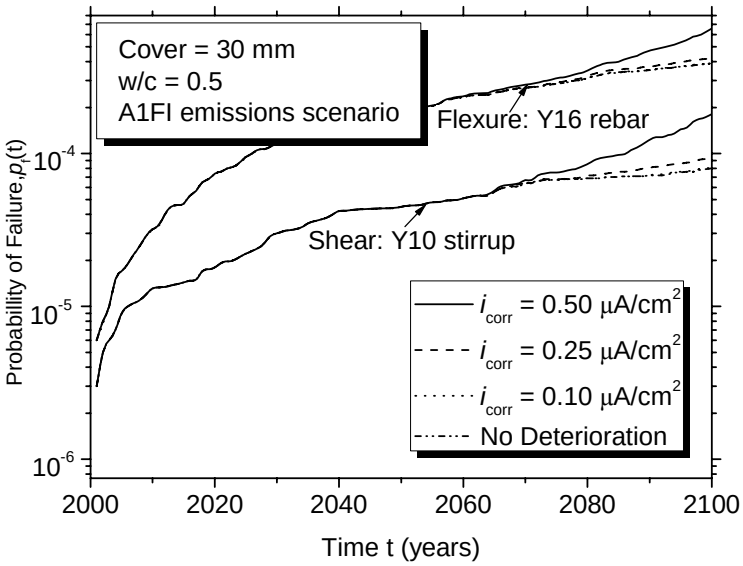

Fig. 8. Probabilities of failure, for various corrosion rates

7.2.6 Proposed increase in design cover

Table 3 shows the mean proportion of corrosion damage in the year 2100 for existing covers under all emission scenarios for i_{corr} = 0.25 μA/cm^2 and Y16 rebar with a w/c of 0.45. In this study, the mean proportion of corrosion damage for the best mitigation scenario is taken as the baseline case. Table 3 then shows proposed covers needed for A1FI and B1 emission scenarios so that their reduced mean proportion of corrosion damage match the baseline case. Fig. 9 shows the proposed increase in design cover needed for A1FI and B1 emission scenarios for various corrosion rates based on w/c=0.45. Therefore, it is found that existing design cover of 55 mm or less would need to increase by approximately 6-18 mm and 3-10 mm under A1FI and B1 emission scenarios for all corrosion rates, respectively. However, if existing design cover exceeds 55 mm then the mean proportion of corrosion damage reaches near zero so there is no need for increases in design cover. It is observed that similar increases in design cover are needed to ameliorate corrosion damage for Y10 and Y27 reinforcement or various water-cement ratios. If the time period is reduced to 2050 (50 years), then a similar analysis used to derive Table 3 and Fig. 9 shows that existing design cover would need to increase by 5 to 16 mm if existing design cover is 35 mm or less. However, if existing design cover exceeds 35 mm then the mean proportion of corrosion damage reaches near zero so there is no need for increases in design cover.

Existing cover (mm)	d_{crack} (w=1 mm, t =100 years)			Proposed cover (mm)	
	A1FI	B1	Best mitigation	A1FI	B1
20	7.23	1.727	0.377	38	31
30	2.127	0.404	0.092	44	36
40	0.367	0.063	0.013	52	46
45	0.089	0.015	0.004	56	49
50	0.023	0.003	0.0	58	52
55	0.006	0.0	0.0	60	55
60	0.0	0.0	0.0	60	60

Table 3. Mean Proportion of Corrosion Damage for Existing Covers under All Emission Scenarios and Proposed Covers for A1FI and B1 Emission Scenarios for i_{corr} = 0.25 μA/cm^2 and Y16 Rebar with a w/c of 0.45

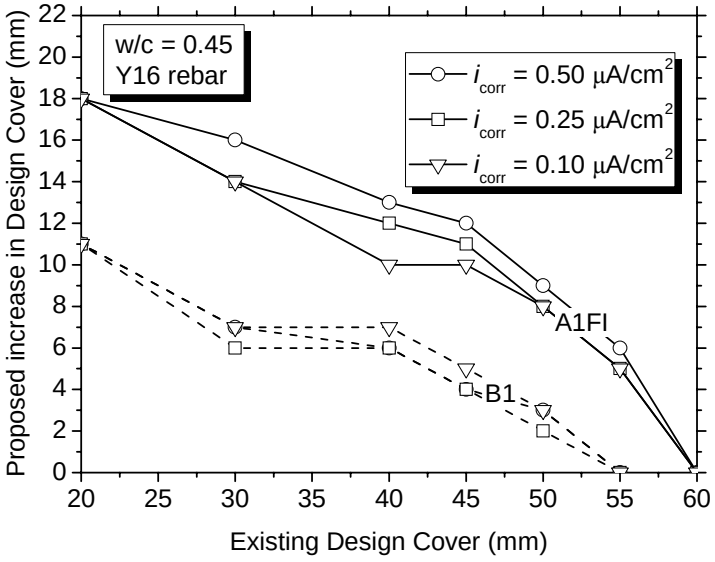

Fig. 9. Proposed increase in design cover for A1FI and B1 emission scenarios and various corrosion rates with a w/c of 0.45

7.2.7 Parameter sensitivity

A sensitivity analysis was conducted to investigate the relative importance of the variability of each random variable on the variability of the corrosion initiation limit state, corrosion damage, and strength limit state functions. In this study, an approach proposed by Melchers and Ahammed (2004)[52] will be used. The responses used in the sensitivity analysis are probability of corrosion initiation (p_{ci}), mean proportion of corrosion damage ($\bar{d}_{crack}$), and

probabilities of flexural and shear failure (p_{fM} and p_{fV}) at 100 years. Results are shown in Table 4.

As seen in Table 4, the time to corrosion initiation is clearly influenced by both concrete cover and concrete compressive strength. For the mean proportion of corrosion damage the following parameters have been identified as the most important: carbonation depth model error (ME_c), corrosion rate, cover and concrete compressive strength. The probability of flexural failure is affected by M_u/M_{nom}, corrosion rate, carbonation depth model error, cover and concrete compressive strength. The probability of shear failure is influenced by V_c/V_{cnom}, V_s/V_{snom}, corrosion rate, carbonation depth model error and cover. In all cases, it is observed that model errors and cover are the parameters most likely to influence structural reliabilities for carbonation-induced corroding RC structures.

Parameters X_i	Absolute Influences			
	I_{Xi} (%) p_{ci}	I_{Xi} (%) $\bar{d}_{crack}$	I_{Xi} (%) p_{fM}	I_{Xi} (%) p_{fV}
Model error (ME_c)	0.0	29.6	16.3	13.2
Concrete compressive strength	33.9	11.5	11.2	7.8
Cover	59.3	14.6	15.4	10.9
Model error (T_{sp})	0.0	4.1	0.0	0.0
CO_2 concentration	6.8	9.6	8.5	3.8
$f_{ct}(t)$	0.0	5.6	0.0	0.0
$E_c(t)$	0.0	5.8	0.0	0.0
Model error (i_{corr})	0.0	14.9	18.0	16.9
δ_0	0.0	4.3	0.0	0.0
M_u/M_{nom}	0.0	0.0	30.6	0.0
V_c/V_{cnom}	0.0	0.0	0.0	23.0
V_s/V_{snom}	0.0	0.0	0.0	23.4

Table 4. Absolute Influence of Various Parameters on the Variability of Probability of Corrosion Initiation, p_{ci}, Mean Proportion of Corrosion Damage, $\bar{d}_{crack}$, and Probabilities of Flexural and Shear Failure, p_{fM} and p_{fV}

8. RELIABILITY OF PRESTRESSED CONCRETE STRUCTURES

8.1 Reduction in area of prestressing steel

Concrete carbonation causes general (uniform) corrosion of prestressing concrete wires and strands resulting in a decrease in performance of PSC bridges.[24] In the case of general corrosion and assuming a constant corrosion rate, the reduction in the radius of a corroding prestressing wire Δr (in mm) at time t is

$$\Delta r = 0.0116 i_{\text{corr}} \left(t - T_{\text{i}} \right) \tag{23}$$

where T_{i} is the time to corrosion initiation (years).

A prestressing strand comprises of seven wires (see Fig. 10) where the radius of each wire is 4.3 mm. It is assumed that only when the carbonation depth reaches the surface of wires does the prestressing steel corrode. If we assume that the corrosion rate is constant for all k prestressing wires of the same radius r. Then the cross-sectional area A_{st} of a prestressing strand after t years of corrosion is

$$A_{\text{st}}(t) = \begin{cases} 7\pi r^2 & 0 \le \text{t} < T_{\text{i}} \\ 3\pi r^2 + 4\pi \left[r - \Delta r(t) \right]^2 & T_{\text{i}} \le \text{t} < r / 0.0116 i_{\text{corr}} \end{cases} \tag{24}$$

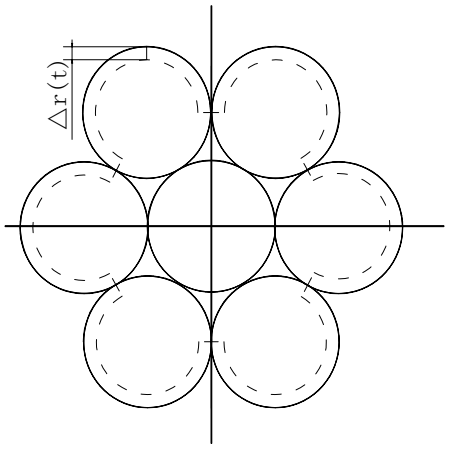

Fig. 10. General corrosion loss model for prestressing strand

8.2 Time-dependent reliability analysis

The ultimate limit state considered in this study is flexural strength. Based on AASHTO LRFD code (1998),[53] the resistance of member R(t) at time t is

$$R(t) = \mathrm{ME} f_{\mathrm{ps}} A_{\mathrm{st}}(t)\left[d_{\mathrm{p}} - 0.5\beta_1 c \right] \tag{25a}$$

where

$$0.85 \geq \beta_1 = 0.85 - 0.05\left(f_{\mathrm{c}} - 28 \right)/7 \geq 0.65 \tag{25b}$$

$$\left(0.85\beta_1 f_{\mathrm{c}} b - k A_{\mathrm{st}}(t) f_{\mathrm{pu}} / d_{\mathrm{p}} \right) c = A_{\mathrm{st}}(t) f_{\mathrm{pu}} \tag{25c}$$

$$f_{\mathrm{ps}} = f_{\mathrm{pu}}\left(1 - kc/d_{\mathrm{p}} \right) \quad k = 2\left(1.04 - f_{\mathrm{py}}/f_{\mathrm{pu}} \right) \tag{25d}$$

where ME is flexural model error; f_{pu} is the ultimate tensile strength of prestressing steel (MPa); f_{ps} is the average stress in prestressing steel (MPa); f_{py} is the yield strength of prestressing steel (MPa); c is the distance between the neutral axis and the compressive face; A_{st} is the area of prestressing steels (mm^2); β_1 and k are the stress block factors; d_{p} is the effective height of cross section (mm); f_{c} is the concrete compressive strength (MPa); and b is the effective width of the compression zone of the cross section when the cross section is I-shaped (mm). Eq. (25a) is appropriate for an I-shaped section for flexural strength limit state with the compression zone is in the top flange. Spatial effects for geometric and physical parameters on structural resistance are not considered for general corrosion as their inclusion will be less important as it is for chloride-induced pitting corrosion.[13] However, inclusion of spatial variability is an area for further research.

The critical limit state is

$$G_{\mathrm{i}}(X) = R(t) - S_{\mathrm{L}}(t) - S_{\mathrm{D}} \tag{26}$$

where R(t) is the resistance at the location of peak flexural action that is close to the middle of the span at time t; S_{L}(t) is the peak live load effect at the location of peak flexural action at time t; and S_{D} is the dead load effect. If it is assumed that k load events takes place within the time interval (0,t) at times t_i (i=1, 2,….k), the cumulative probability of structural failure of service proven structures anytime during the time interval (0,t) is

$$p_{\mathrm{f}}(t) = 1 - \Pr(G_1 > 0 \cap G_2 > 0 \cap \cdots \cap G_{\mathrm{k}} > 0) \tag{27}$$

where G_{i} is the limit state function at time t.

8.3 Illustrative example – PSC bridge girder

8.3.1 Structural configuration

The bridge considered in this study is a typical simple span PSC bridge, which has a span of 20 m and clear roadway width of 8.4 m. The bridge consists of four precast prestressed AASHTO Type IV girders (see Fig. 11) with spacing of 2.3 m and a 200 mm thick cast-in-place concrete deck. The girder was designed according to the AASHTO LRFD Bridge Design Specification (2004)[54] assuming bonded tendons, unshored construction and no composite action between the girder and the cast-in-place slab. The specified concrete compressive strength is 30 MPa, water-cement ratio is 0.5 and nominal ultimate tensile strength of the prestressing steel (f_{pk}) is 1860 MPa. A total of 26 7-wires strands were required to carry the total design loads. Six centrally located strands (positioned in three rows) are harped near the support used for resist shear force and only twenty strands remain horizontal in two levels of ten strands each. Cover concrete for prestressing strands are 20 mm (level 1), 70 mm (level 2) and 120 mm (level 3). For Most existing PSC bridges built in 1970~1980's in China, nominal concrete cover (C_{bnom}) is about 20 mm due to poor construction.

Three different components of dead load are considered: precast concrete, cast-in-place deck and 80 mm asphalt overlay. Axle spacing and distribution of axle loads are calculated based on a US HS-20 truck and the truck is located on the bridge to cause peak flexural actions.[55] The service life of the structure considered in this study is taken as 100 years.

For two lane bridges, the critical load effect usually occurs when two heavily loaded trucks are side by side and have fully correlated weights.[56] It is assumed that the number of fully correlated trucks is 600 trucks/year.[56] A summary of statistical parameters representative of PSC bridge girders in China is given in Table 2 and Table 5. Prestress loss is not herein considered for the strength limit state, although it is relevant for serviceability performance.

Parameters	Mean	COV	Distribution	References
f_{pu} (MPa)	1.04 f_{pk}	0.025	Normal	[57]
C_b bottom cover	C_{bnom}	0.15	Normal	[58]
D beam depth (mm)	D_{nom}	0.002	Normal	[58]
Flexure (ME)	1.01	0.046	Normal	[59]
D_1 Dead load due to precast concrete	1.03 D_n	0.08	Normal	[60]
D_2 Dead load due to concrete road deck	1.05 D_n	0.10	Normal	[60]
D_3 Dead load due to asphalt overlay	80 mm	0.25	Normal	[60]
w single truck load (kN)	240	0.40	Normal	[61]
Impact factor (IF)	1.15	0.10	Normal	[61]
Girder distribution factor	λ^a= 0.93	0.12	Normal	[62]

a, bias factor

Table 5. Statistical parameters for PSC bridge girder.

8.3.2 Computational procedure

The Monte-Carlo event-based simulation analysis considers the variability and uncertainties of environments loads, material properties, dimensions and deterioration processes. For each simulation run the time to corrosion initiation for each layer of strands is calculated. Note that CO_2 concentration is fully correlated with time. At each time increment, the loss of the wire radius and peak live load is generated. Note that corrosion of each wire in each strand is fully correlated. The cross-sectional area is then inferred. The resistance of the strands is calculated from Eqs. (25). Flexural action is calculated for the cross-section at the location of peak flexural action. Failure is deemed to occur if the flexural action exceeds the structural resistance at the cross-sections. Hence time-dependent failure probabilities can be evaluated from Eqs. (26) and (27). The design lifetime of bridge is 100 years, hence failure probabilities are calculated for 100 successive annual time increments. In the results to follow the time interval t_i to t_{i+1} is taken as 1 year. In the present case, 10 million simulation runs are used to calculate the failure probabilities.

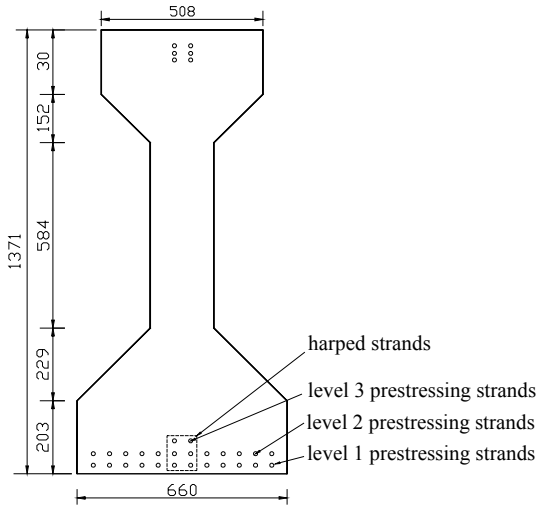

Fig. 11. AASHTO type IV bridge girder at mid-span

8.3.3 Results

Using the CO_2 concentration models in Fig. 1, the mean carbonation depths under ambient environments for the three scenarios are 20.2, 14.3, and 12.1 mm after 100 years, respectively. The COV for carbonation depth increases with time from 0.20 to 0.22. For the worst case scenario (A1FI) the carbonation depth is 53% higher than that for the best mitigation scenario. This shows that future emission scenarios induced by economic development and population growth affects concrete carbonation and thus the onset of corrosion of prestressing steels.

Table 6 shows the probabilities of corrosion initiation in the year 2100 for existing covers under all emission scenarios with a w/c of 0.45. In this study, the probabilities of corrosion initiation for the best mitigation scenario is taken as the baseline case. Table 6 then shows proposed covers needed for A1FI and B1 emission scenarios so that their probabilities of corrosion initiation match the baseline case. Therefore, it is found that existing design cover for new bridges of 50 mm or less would need to increase by approximately 10-15 mm and 3-5 mm under A1FI and B1 emission scenarios, respectively. However, if existing design cover exceeds 50 mm then the probability of corrosion initiation reaches near zero so there is no need for increases in design cover.

Existing cover, mm	p_{ci} (100)			Proposed cover, mm	
	A1FI	B1	Best mitigation	A1FI	B1
20	0.2054	0.04151	0.01032	34	23
30	0.0362	0.00464	0.000992	42	33
40	0.00187	0.00012	0.00002	52	43
45	0.000261	0.00001	0.000002	55	49
50	0.000031	0.000001	0.0	60	55
55	0.000002	0.0	0.0		
60	0.0	0.0	0.0		

Table 6. Probabilities of corrosion initiation for existing covers under all emission scenarios and proposed covers for A1FI and B1 emission scenarios with a w/c of 0.45

Fig. 12 shows the probabilities of failure for PSC bridges. For the first 70-80 years of service life the effect of carbonation on structural reliability is negligible. However, for the worst case scenario (A1FI) the probability of failure is 10% higher than that observed for the best mitigation scenario. It was found that corrosion induced by carbonation will result in a negligible increase in probability in failure of PSC bridge girders when the concrete cover is increased to 40 mm.

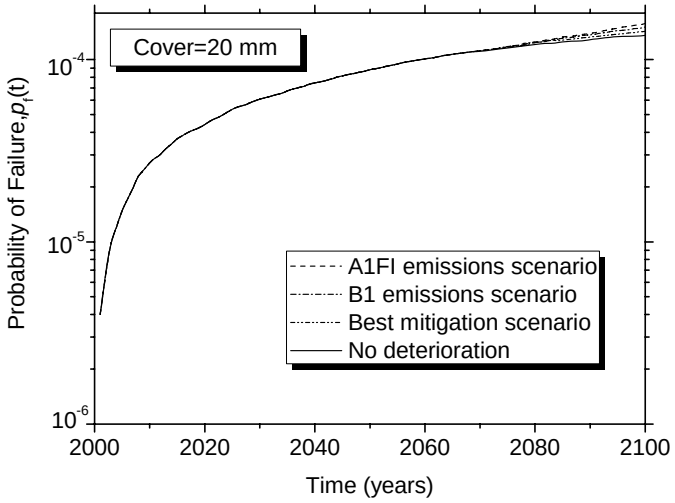

Fig. 12. Time-dependent probabilities of failure

9. CONCLUSIONS

The influence of ambient exposure and time-dependent increases in CO_2 concentration have been incorporated into probabilistic carbonation deterioration models. Consequently, a time-dependent reliability analysis has been developed to calculate probabilities of corrosion initiation, mean proportions of corrosion damage and probabilities of structural collapse when the CO_2 concentration increases with time over the next 100 years. A reliability analysis of RC structures including various emission and mitigation scenarios found that the probability of corrosion initiation is up to 720% higher than a scenario based on maximum mitigation of CO_2 emissions. It was also found that the worst emissions scenario increased the likelihood and extent of corrosion damage by 540% when compared to the structural reliability for the best mitigation scenario. For the worst case scenario and 1 mm crack width the mean proportion of corrosion damage was observed to be only 0.3% for good durability design specification. If the worst emissions scenario is viewed as the most likely scenario, and existing design cover is less than 50-60 mm, then increasing design cover for RC and PSC structures by approximately 3-18 mm may be needed to ameliorate corrosion damage over the next 100 years. It was also found that for the worst emissions scenario the probability of shear failure is 18% higher than for the best mitigation scenario and the probability of flexural failure is only 6% higher than that predicted for the best mitigation scenario. For PSC structures, a reliability analysis also found that for the worst case scenario the probability of failure is about 10% higher than that for the best mitigation scenario.

ACKNOWLEDGEMENTS

The financial support of Department of Hunan Provincial Communications, China under Grant 200 617 and the China Scholarship Council are gratefully acknowledged. This work was undertaken while the first author was a visitor to the Centre for Infrastructure Performance and Reliability at The University of Newcastle. The facilities and support provided by the Centre for Infrastructure Performance and Reliability are much appreciated. The support of the Australian Research Council is also gratefully acknowledged.

REFERENCES

[1] Mehta P. K. and Monteiro P. J. M. *Concrete microstructure, properties and materials*. first (ed.), Indian Concrete Institute, Chennai, India. 1997.

[2] Mori Y. and Ellingwood B. R. Reliability-based service-life assessment of aging concrete structures. *Journal of Structural Engineering, ASCE,* 1993, 119(5), 1600-1621.

[3] Vu K. A. T. and Stewart M. G. Structural reliability of concrete bridges including improved chloride-induced corrosion models. *Structural Safety*, 2000, 22(4), 313-333.

[4] Estes A. C. and Frangopol D. M. Bridge lifetime system reliability under multiple limit states. *Journal of Bridge Engineering, ASCE,* 2001, 6(6), 523-528.

[5] Frier C. and Sorensen J. D. Stochastic analysis of the multi-dimensional effect on chloride ingress into reinforced concrete. *ICASP10 Applications of Statistics and Probability in Civil Engineering*, J. Kanda, T. Takada, H. Furuta (eds.), Taylor &Francis, London, (CD-ROM), 2007.

[6] Li Y., Vrouwenvelder T., Wijnants G. H. and Walraven J. Spatial variability of concrete deterioration and repair strategies. *Structural Concrete,* 2004, 5(3), 121-130.

[7] Vu K. A. T. and Stewart M. G. Predicting the likelihood and extent of RC corrosion-induced cracking. *Journal of Structural Engineering, ASCE*, 2005, 131(11), 1681-1689.

[8] Stewart M. G. and Mullard J. A. Spatial time-dependent reliability analysis of corrosion damage and the timing of first repair for RC structures. *Engineering Structure,* 2007, 29(7), 1457-1464.

[9] Sudret B., Defaux G. and Pendola M. Stochastic evaluation of the damage length in RC beams submitted to corrosion of reinforcing steel. *Civil Engineering and Environmental Systems*, 2007, 24(2), 165-178.

[10] Stewart M. G. Spatial variability of pitting corrosion and its influence on structural fragility and reliability of RC beams in flexure. *Structural Safety*, 2004, 26(4), 453-470.

[11] Val D. V. Deterioration of strength of RC beams due to corrosion and its influence on beam reliability. *Journal of Structural Engineering, ASCE*, 2007, 133(9), 1297-1306.

[12] Stewart M. G. and Al-harthy A. Pitting corrosion and structural reliability of corroding RC structures: Experimental data and probabilistic analysis. *Reliability Engineering and System Safety,* 2008, 93(3), 373-382.

[13] Stewart M. G. Mechanical behaviour of pitting corrosion of flexural and shear reinforcement and its effect on structural reliability of corroding RC beams. *Structural Safety*, 2009, 31, 19-30.

[14] Marsh P. S. and Frangopol D. M. Reinforced concrete bridge deck reliability model incorporating temporal and spatial variations of probabilistic corrosion rate sensor data. *Reliability Engineering and System Safety*, 2008, 93(3), 394-409.

[15] Peng J. and Stewart M. G. Climate change, deterioration and time-dependent reliability of concrete structures. *Proceeding of 20th Australasian Conference on the Mechanics of Structures and Materials,* Toowoomba, Queensland, 2008. (in press).
[16] Stewart M. G. and Rosowsky D. V. Structural safety and serviceability of concrete bridges subject to corrosion. *Journal of Infrastructure Systems, ASCE*, 1998, 4(4), 146-155.

[17] Meehl G. A., Stocker T. F., Collins W. D., Friedlingstein P., Gaye A. T., Gregory J. M., Kitoh A., Knutti R., Murphy J. M., Noda A., Raper S. C. B., Watterson I. G., Weaver A. J., and Zhao Z.-C. "Global climate projections." In: Climate Change 2007: The Physical Science Basis. Contribution of Working Group I to the Fourth Assessment Report of the Intergovernmental Panel on Climate Change [S. Solomon, D. Qin, M. Manning, Z. Chen, M. Marquis, K. B. Averyt, M. Tignor and H. L. Miller (eds.)]. Cambridge University Press, Cambridge, United Kingdom and New York, NY, USA, 2007, 789-812.

[18] Yoon I. S., Çopouroğlu O. and Park K. B. Effect of global climatic change on carbonation progress of concrete. *Atmospheric Environment*, 2007, 41, 7274-7285.

[19] Stewart, M. G. Spatial variability of damage and expected maintenance costs for deteriorating RC structures. *Structure and Infrastructure Engineering*, 2006, 2(2), 79-90.
.
[20] Engelfried R. Preventive prevention by low permeability coatings. *Proceeding of the Concrete Society Conf. on Permeability of Concrete and its Control*, London, 1985, 107-117.

[21] CEB. *New approach to durability design – an example for carbonation induced corrosion*. In: Schiessl, P. (ed.), Bulletin, 238, Comite Euro-International du Beton, Lausanne, 1997.

[22] Kersner Z., Teply B. and Novk D. Uncertainty in service life prediction based on carbonation of concrete. Proceeding of the 7th International Conference on Durability of Building Materials and Components, C. Sjostrom(ed.), E&FN Spon, London, 1996, 13-30.

[23] Papadakis V. G., Fardis M. N. and Vayenas G. G. Effect of composition, environmental factors and cement-lime coating on concrete carbonation. *Material and Structure*, 1992, 25, 293-304.

[24] Coronelli D. and Gambarova P. Structural assessment of corroded reinforced concrete beams: modeling guidelines. *Journal of Structural Engineering, ASCE*, 2004, 130(8), 1214-1224.

[25] Parameswaran L., Kumar R. and Sahu G. K. Effect of carbonation on concrete bridge service life. *Journal of Bridge Engineering, ASCE*, 2008, 13(1), 75-82.

[26] Bolzoni F., Fumagalli G., Lazzari L., Ormellese M. and Pedeferrim. P. *Mixed–in inhibitors for concrete structures*. European Federation of Corrosion Publications Number 38: Corrosion of reinforcement in concrete, mechanisms, monitoring, inhibitors and rehabilitation

techniques, Edited by Raupach, M., Elsener, B., Polder, R. and Mietz, J.. ISSN: 1354-5116, 2007, 199-201.

[27] Duracrete. *Probabilistic performance based durability design of concrete structures - statistical quantification of the variables in limit state functions*. The European union-Brite EuRam III, Project BE 95-1347, 2000, 75-96.

[28] Heiyatuduwa R., Alexander M. G. and Mackechinie J. R. Performance of a penetrating corrosion inhibitor in concrete affected by carbonation-induced Corrosion. *Journal of Material in Civil Engineering*, 2006, 18(6), 842-850.

[29] Xu Y. M., She H. L. and Miksic B. A. Comparison of inhibitors MCI and NaNO2 in Carbonation-induced Corrosion. *Material Performance*, 2004, 42, 42-46.

[30] Weyers R. E. Service life model for concrete structures in chloride-laden environments. *ACI Materials Journal*, 1998, 95(4), 445-453.

[31] El Maaddawy T. and Soudki K. A model for prediction of time from corrosion initiation to corrosion cracking. *Cement & Concrete Composite*, 2007, 29, 168-175.

[32] Liu Y. and Weyers R. E. Modeling the time-to-corrosion cracking in chloride contaminated reinforced concrete structures. *ACI Materials Journal*, 1998, 95(6), 675-680.

[33] Chernin L. and Val D. V. Prediction of cover cracking in reinforced concrete structures due to corrosion. *MEDACHS 08: 1st International Conference on Construction Heritage in Coastal and Marine Environments*, 28-30 January, Lisbon (CD-ROM), 2008.

[34] A23.3-94. *Design of concrete structures*. Canadian Standards Association, Rexadle, ON, Canada, 1994.

[35] Thoft-Christensen P. *Stochastic modelling of the crack initiation time for reinforced concrete structures*. ASCE Structures Congress, Philadelphia, May 8-10, 2000, 8.

[36] Vu K. A. T., Stewart M. G. and Mullard J. A. Corrosion-induced cracking: experimental data and predictive models. *ACI Structural Journal*, 2005, 102(5), 719-726.

[37] Vidal T., Castel A. and Francois R. Analyzing crack width to predict corrosion of reinforced concrete. *Cement and Concrete Research*, 2004, 34, 165-174.

[38] Al-Harthy A. S., Mullard J. and Stewart M. G. Cracking in concrete due to corrosion of steel reinforcement. *The Proceeding of 5th International Conference on Concrete under Severe Conditions, Environment and Loading*, F. Toutlemonde (ed.), 2007, 383-390.

[39] ACI 318. *Building code requirements for structural concrete*. Detroit, Michigan, 2005.

[40] Nowak A. S., Szerszen M. M., Szeliga E. K., Szwed A. and Podhorechi P. J. *Reliability-based calibration for structural concrete*. Report No. UNLCE 05-03, Department of Civil Engineering, University of Nebraska, 2005.

[41] Ellingwood B. R., Galambos T. V., MacGegor J. G. and Cornell C. A. *Development of a probability based load criterion for American National Standard A58*. National Bureau of Standards Special Publication 577, US Government Printing Office, Washington, D C, 1980.

[42] Ellingwood B. R. and Culver C. G. Analysis of live loads in office buildings. *Journal of the Structural Division, ASCE*, 1977, 103(ST8), 1551–1560.

[43] Philpot T. A, Rosowsky D. V. and Fridley K. J. Serviceability design in LRFD for wood. *Journal of Structural Engineering, ASCE*, 1993, 119(12), 3649–3667.

[44] ANSI/ASCE 7-93. *Minimum design loads for buildings and other structures*. New York, ASCE, 1994.

[45] BS 8110-1. *Structural use of concrete - Part 1: Code of practice for design and construction*. BSI, UK, 1997.

[46] BS EN 1992-1-1. *Eurocode 2: Design of concrete structures - Part 1-1: General rules and rules for buildings*. UK, 2004.

[47] AS3600. *Concrete structures.* Standard Association Australia, Homebush, New South Wales, Australia, 2001.

[48] GB50010. *Code for design of concrete structures*. China Design Standard Committee, Beijing, 2002.

[49] Stewart M. G. Workmanship and its influence on probabilistic models of concrete compressive strength. *ACI Materials Journal*, 1995, 92(4), 361-372.

[50] Mirza S. A. and MacGregor J. G. Variations in dimensions of reinforced concrete members. *Journal of the Structural Division, ASCE*, 1979, 105(ST4), 751-766.

[51] Mirza S. A., Hatzinikolas M. and MacGregor J. G. Statistical descriptions of strength of concrete. *Journal of the Structural Division, ASCE*, 1979, 105(ST6), 1021-1037.

[52] Melchers R. E. and Ahammed M. A fast approximate methods for parameter sensitivity estimation in Monte-Carlo structural reliability. *Computers and Structures*, 2004, 82, 55-61.

[53] AASHTO. *AASHTO LRFD bridge design specification*. Washington D C: AASHTO, 1998.

[54] AASHTO. *AASHTO LRFD bridge design specification*. Washington D C: AASHTO, 2004.

[55] Darmawan M. S. and Stewart M. G. Spatial time-dependent reliability analysis of corroding pretensioned prestressed concrete bridge girders. *Structural Safety*, 2007, 29, 16-31.

[56] Nowak A. S. Live load model for highway bridges. *Structural Safety*, 1993, 13(1), 53–66.

[57] Mirza S. A, Kikuchi D. K. and MacGregor J. G. Flexural strength reduction factor for bonded prestressed concrete beams. *ACI Materials Journa*l, 1980, 77(4), 237-246.

[58] Design Standard. *Structural reliability-based design for highway engineering*. Beijing: China Planning Press, 1999.

[59] Ellingwood B., Galambos T. V., MacGregor J. G. and Cornell C. A. Development of a probability-based load criterion for American National Standard A58, *National Bureau of Standards Special Publication No. 577,* Washington, D.C., 1980.

[60] Nowak A. S., Park C. and Casas J. R. Reliability analysis of prestressed concrete bridge girders: comparison of euro code, Spanish Norma IAP and AASHTO LRFD. *Structural Safety,* 2001, 23, 331-344.

[61] Nowak A. S. and Grouni H. N. Calibration of the OHBDC -1991. *Canadian Journal of Civil Engineering*, 1994, 21,22–35.

[62] Hwang E-S. and Nowak A. S. Simulation of dynamic load for bridges. *Journal of Structural Engineering, ASCE*, 1991, 117(5), 1413-1434.

THE UNIVERSITY OF NEWCASTLE

SCHOOL OF ENGINEERING

CIVIL, SURVEYING AND ENVIRONMENTAL ENGINEERING

RESEARCH REPORTS

This report is one of a continuing series of Research Reports published by Civil, Surveying and Environmental Engineering at the University of Newcastle. An abridged list of recently published titles in this series is provided below. Requests for a more detailed list and/or copies of other reports should be addressed to:

The Secretary
Civil, Surveying and Environmental Engineering
The University of Newcastle
University Drive
CALLAGHAN NSW 2308

Telephone: (02) 4921 6058
Facsimile : (02) 4921 6991

REPORT NO.	ISBN NO.	TITLE AND AUTHOR
265.04.2008	9781 9207 01 96 3	Assessing The Costs And Benefits Of United States Homeland Security Spending M.G. Stewart and J. Mueller
266.04.2008	9781 9207 01 97 0	Assessing The Risks, Costs And Benefits Of Australian Aviation Security Measures M.G. Stewart and J. Mueller
267.04.2008	9781 9207 01 98 7	Assessing The Risks, Costs And Benefits Of United States Aviation Security Measures M.G. Stewart and J. Mueller
268.08.2008	9781 9207 01 99 4	Structural Reliability Analysis Of Reinforced Grouted Concrete Block Masonry Walls In Compression Designed To Chinese Code GB 50003 X.M. Zhai and M.G. Stewart
269.11.2008	9780 9805 0354 8	Reinforcement Corrosion Initiation and Activation Times In Concrete Structures Exposed To Severe Marine Environments R.E. Melchers and C.Q. Li

270.11.2008	9780 9805 0355 5	Carbonation-Induced Corrosion Damage and Structural Safety For Concrete Structures Under Enhanced Greenhouse Conditions J. Peng and M.G. Stewart